Remote Sensing Applications: Society and Environment 35 (2024) 101252

Contents lists available at ScienceDirect

Remote Sensing Applications: Society and Environment

journal homepage: www.elsevier.com/locate/rsase

Comparison of functional and structural biodiversity using Sentinel-2 and airborne LiDAR data in agroforestry systems

Xi Zhu [a,*], Mila Luleva [a], Sebastian Paolini van Helfteren [a], Yaqing Gou [a], Weronika Gajda [b], Elnaz Neinavaz [c]

[a] Remote Sensing, Rabobank, Croeselaan 18, Utrecht, 3521 CB, The Netherlands
[b] Department of Information and Computing Sciences, Utrecht University, Princetonplein 5, Utrecht, 3584 CC, The Netherlands
[c] Natural Resources, Faculty Geo-Information Science and Earth Observation, University of Twente, Hallenweg 8, Enschede, 7522 NH, The Netherlands

ARTICLE INFO

Keywords:
Functional biodiversity
LiDAR
Sentinel-2
Structural biodiversity
Agroforestry

ABSTRACT

Biodiversity plays a critical role in maintaining the health and stability of ecosystems. Biodiversity monitoring has traditionally been labor-intensive, prompting a shift towards remote sensing techniques for efficient and large-scale approaches. In this research, we explore the use of Sentinel-2 satellite data and airborne LiDAR data to evaluate and compare functional and structural biodiversity in agroforestry areas within two distinct ecoregions, namely the Montane forests ecoregion and the Victoria Basin forest-savanna mosaic ecoregion in Columbia and Tanzania, respectively. The aim of the study is to compare functional diversity and structural diversity across varying spatial scales and land cover types including trees, cropland and grassland, thereby addressing the correlation and divergence between functional and structural diversity in different ecological contexts. Our methodology involves integrating airborne LiDAR data to assess structural diversity and Sentinel-2 data to estimate functional diversity based on the proxies of three key functional traits, leaf chlorophyll content (CHL), leaf anthocyanin content (ANTH), and specific leaf area (SLA). We developed two novel functional diversity indices, ShannonF and GiniF, which are modified versions of the well-established Shannon index and Gini index. These novel indices effectively incorporate both functional richness and evenness into their calculations. Our results indicated a significant correlation between our proposed ShannonF index and Shannon index derived from LiDAR, with stronger correlations at larger spatial scales. This study demonstrated that trees exhibit higher biodiversity than grassland and cropland across both study areas, with particularly high biodiversity in Colombia's Montane forests ecoregion. These findings underscore the potential of integrating satellite and airborne LiDAR data for comprehensive biodiversity assessment in agroforestry systems, offering valuable insights for global ecosystem management and conservation efforts.

1. Introduction

Biodiversity is vital for preserving existing ecosystems on Earth. It is essential for maintaining healthy ecosystem function, as it enhances productivity and resilience in the face of human disturbance (Wang and Gamon, 2019). From an instrumental perspective, biodiversity enhances and sustains essential ecosystem functions such as nutrient and energy fluxes, and ecosystem services such

* Corresponding author.
E-mail address: xi.zhu@gmail.com (X. Zhu).

https://doi.org/10.1016/j.rsase.2024.101252
Received 22 March 2024; Received in revised form 8 May 2024; Accepted 21 May 2024
Available online 24 May 2024

as resource production and increase in resiliency (Cardinale et al., 2012; Rands et al., 2010). In addition, biodiversity has cultural, recreational and ethical values (Laurila-Pant et al., 2015).

When considering the species biodiversity of a ecosystem, two fundamental aspects are the species richness and species evenness (Hamilton, 2005). Species richness is the number of species within the community, and species evenness assesses the distribution of the number of individuals of each of these species (Ma, 2005). Traditional monitoring of species biodiversity through field work has been considered costly and labor-intensive; hence there is a growing interest in exploring remote sensing techniques for efficient monitoring and quantifying of biodiversity (Toledo et al., 2001; Félix et al., 2018). Monitoring biodiversity dynamics using satellite data provides further insights into understanding biodiversity change caused by anthropogenic activities, allowing us to act promptly (Makino et al., 2020). At a regional scale, airborne LiDAR and hyperspectral data provide detailed structure and spectral information for individual tree species mapping (Wallis et al., 2023; Zheng et al., 2023). Towards a global scale, satellite data such as ESA's Sentinel-2 offer the opportunity to map species diversity (Shi et al., 2018; Zhao et al., 2018) and its changes frequently, at an acceptable spatial resolution and cost. Sentinel-2 data offer a good potential for biodiversity mapping thanks to the global coverage with a medium spatial resolution to map diversity at fine to large scales, a moderate spectral resolution relevant to derive vegetation indices as proxies for physiological traits, and a high temporal resolution allowing for the change detection for biodiversity (Helfenstein et al., 2022). Its application in biodiversity has been demonstrated in many studies (Hauser et al., 2021; Helfenstein et al., 2022; Ma et al., 2019).

In contrast to studying species diversity alone, functional and structural diversity as measures for ecosystem biodiversity are now becoming a subject of interest among a growing number of researchers (Makino et al., 2020; Liu et al., 2023). Functional diversity in flora is usually characterized by the richness and evenness of plant functional traits (Zheng et al., 2023). These traits encompass specific morphological, physiological, phenological, or reproductive properties exhibited by plants (Wang and Gamon, 2019). As plant functional traits do not function in isolation, they form an integrated system where multiple traits interact to determine a plant's overall environmental performance. Consequently, many studies have shifted their focus towards mapping functional diversity by considering multiple traits (Félix et al., 2018; Makino et al., 2020). The literature review revealed that functional diversity richness and evenness have been measured by applying different approaches (Rocchini et al., 2018; Helfenstein et al., 2022). For instance, functional richness, which represents the amount of trait space filled by the species in a community, can be measured by the volume or area (e.g., Convex hull volume) occupied by the considered species in the trait space (Hauser et al., 2021). Convex hull volume indicates the niche extent of the occupied functional space, which makes it affected by extreme values. Functional evenness provides information concerning how evenly traits are distributed in terms of spacing among similar sample points in functional space (Xi et al., 2023). Both functional richness and evenness are crucial components of biodiversity, and their importance is interlinked in determining the overall health, resilience, and functioning of the ecosystem (Ilangakoon et al., 2021; Schneider et al., 2023).

Another aspect of biodiversity is the structural diversity. Structural diversity relates to the physical 3D structure of vegetation within an ecosystem, whereby a richer structural diversity is associated with a larger potential occupancy for different niche spaces (Hauser et al., 2021). In this respect, LiDAR (Light Detection and Ranging) has emerged as an active remote sensing sensor for assessing and quantifying structural diversity, particularly in forest ecosystems (LaRue et al., 2023; Schneider et al., 2017). This active remote sensing technique has been used successfully in estimating canopy height and canopy height profiles with high accuracy compared to field measurement (Mura et al., 2015). Structural diversity is commonly evaluated through canopy height complexity, typically assessed using the Shannon index calculated from the canopy height model (CHM) (Schneider et al., 2017; Listopad et al., 2015). Shannon index considers both structural richness and evenness in its computation.

Functional diversity and structural diversity measure different aspects of biodiversity and are both important for assessing ecosystem diversity. However, it remains unclear how these two aspects of diversity correlate and compare with each other in different spatial scales and different ecoregions, especially in agroforestry areas. Although remote sensing has been widely used in biodiversity assessment in forest areas (Palmroos et al., 2023; Silveira et al., 2021), its application in agroforestry areas remains comparatively underexplored. Agroforestry systems have unique vegetation characteristics due to the combination of different trees and crops (Pantera et al., 2021). The agroforestry areas in this research are within two separate ecoregions, namely the Montane forests ecoregion and the Victoria Basin forest-savanna mosaic ecoregion (Olson et al., 2001) in Columbia and Tanzania with unique characteristics. Studying and comparing the functional and structural diversity can help understand how these variables can be used to provide important information about biodiversity in different ecoregions.

Further, we introduce a novel functional diversity index that combines both functional richness and evenness. We compare the diversity index at different spatial scales within two distinct ecoregions, each encompassing multiple land cover types (i.e., trees, grassland and cropland). Specifically, we assess the biodiversity measures derived from the proposed functional diversity index across various land cover types and ecoregions in agroforestry areas and the scale dependency of the correlation between functional diversity and structural diversity.

2. Study area and data

2.1. Study area

The first study area is located in the Victoria Basin forest-savanna mosaic ecoregion (Olson et al., 2001) which belongs to the tropical and subtropical grasslands, savannas, and shrublands in the United Republic of Tanzania (Fig. 1). It covers an area of approximately 22.87 km^2. The elevation of this ecoregion ranges between 800 m and 1500 m. The climate of this ecoregion is tropical with an annual maximum mean temperature ranging from 24° to 27°, and a minimum mean temperature ranging from 15°

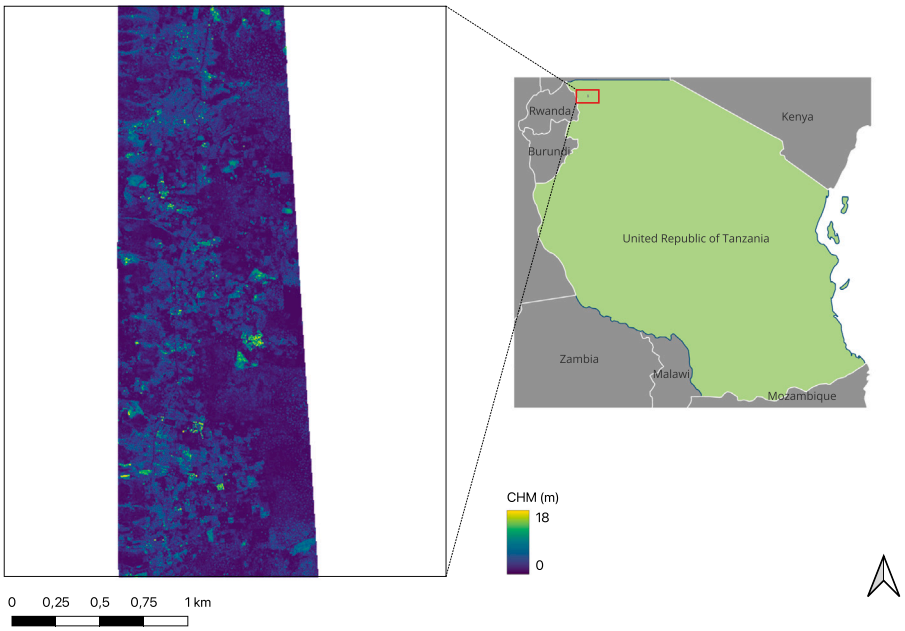

Fig. 1. Airborne LiDAR data coverage of the Victoria Basin forest-savanna mosaic ecoregion, Tanzania.

to 18°. The total annual precipitation ranges from 1000 mm to 1400 mm. The predominant ecosystem consists of extensive areas of savanna and woodland, mixed with small areas of forest (Burgess et al., 2004). The main plant communities include Lake Victoria drier semi-evergreen Guineo-Congolian rain forest, transitional rain forest, moist Combretum wooded grassland, dry Combretum wooded grassland, Evergreen and semi-evergreen bushland and thicket, Edaphic wooded grassland, and swamp forest (van Breugel et al., 2015).

The second study area is located in the Cauca Valley Montane forests ecoregion (Olson et al., 2001), which belongs to the tropical and subtropical moist broadleaf forests biome in Colombia (Fig. 2). It covers an area of approximately 80 km^2. The elevation of this ecoregion ranges between 1000 m and 3000 m. The annual mean temperature ranges from 19.5° to 20.3°, and the total annual precipitation is around 2300 mm. The Cauca Valley Montane forests contains diverse vegetation, including dry areas in the east and humid forests in the middle and upper western slopes (Kattan, 2018). Below 1500 m, the dominant species are Fabaceae and Moraceae. Between 1500 m and 3000 m, the majority of species are in the Lauraceae, Melastomataceae and Rubiaceae families. Above 3000 m, Ericaceae and Asteraceae are the dominant families (Kattan, 2018).

2.2. LiDAR data

The airborne LiDAR campaign was carried out in November 5, 2022 in Tanzania. A Riegl 780i (RIEGL) was used for the campaign. The sensor operates at the wavelength of 1064 nm with a beam divergence of 0.25 mrad. The flying altitude was approximately 700 m above ground with a flying speed of 204 km/h, which resulted a point density of around 20 pts/m^2. The LiDAR flight campaign in Colombia was conducted in October 5, 2022. The sensor used was an Optech Gemini (DirectIndustry) with a wavelength of 1064 nm and a beam divergence of 0.3 mrad. The flying altitude was approximately 600 m above ground with an average speed of 220 km/h, which resulted in an average point density above 30 pts/m^2.

The point cloud data contain coordinates, intensity, return number, number of returns and GPS timestamps of the return. The Point Data Abstraction Library (Butler et al., 2021) was used to classify ground returns from non-ground returns. A digital elevation model (DEM) was generated based on the ground returns, which was then used to normalize all return heights. After normalization, the z value of each point indicated the height from the ground to that point (Zhu et al., 2018). A canopy height model (CHM) was then generated based on the normalized point cloud (Fig. 3). We generated CHMs of 1 m resolution for both sites to harmonize the differences, although the density in the Colombia site allowed for a generation of a higher resolution CHM. This made sure the quality of the CHMs of the two regions are comparable. The LiDAR-derived CHM was down-sampled to the 10 m resolution of Sentinel-2 data.

2.3. Sentinel-2 data

Sentinel-2 images of bottom-of-atmosphere reflectance were acquired in the dry period in June and July of 2022 for the Tanzania site and the Colombia site respectively. The Sentinel-2 Multispectral Imager (MSI) has 13 bands in the visible, near infrared, and

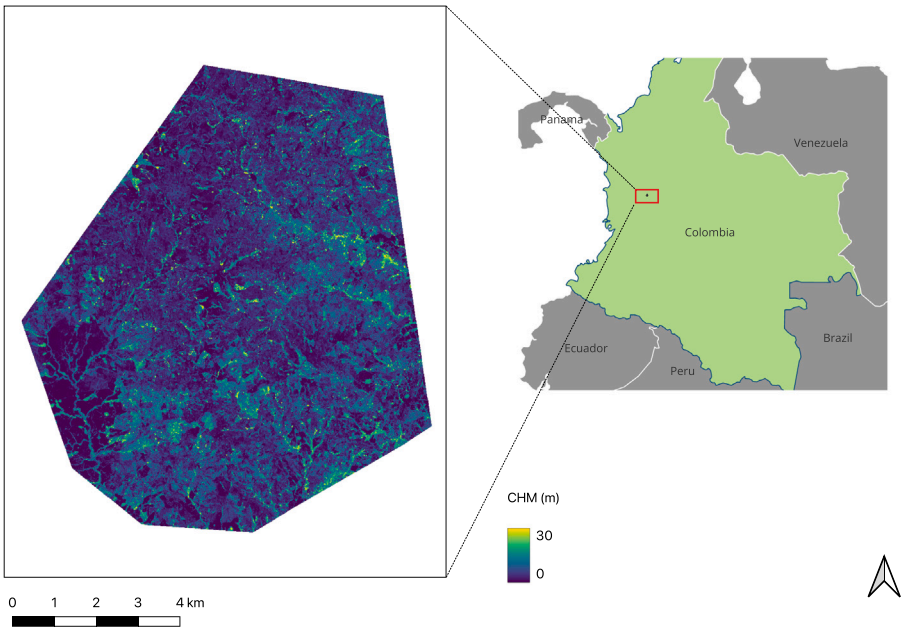

Fig. 2. Airborne LiDAR data coverage of the Cauca Valley Montane forests, Colombia.

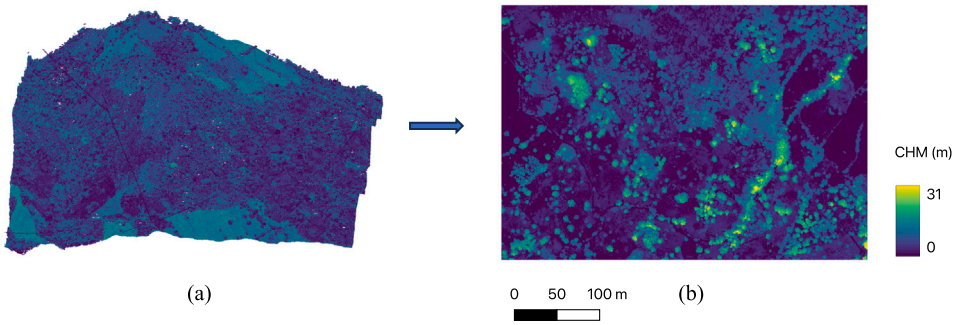

Fig. 3. An example of airborne LiDAR data processing: (**a**) Raw point cloud colorized by intensity, (**b**) Generated CHM colorized by height.

short-wave infrared domains (Drusch et al., 2012). The cirrus band (B10) was excluded as it does not contain any bottom-of-atmosphere information (Richter et al., 2011). Cloud and shadow were masked based on s2cloudless (Zupanc, 2017) and scene classification (Main-Knorn et al., 2017). A median value of each pixel with a resolution of 10 m was taken for multiple sentinel images to create an image composite (Svoboda et al., 2022).

2.4. Land cover map

The Dynamic World land use land cover map featuring nine land cover classes (Brown et al., 2022) was used to mask out non-vegetation bodies. This facilitates the analysis of biodiversity differences among different land cover types (e.g., trees, cropland and grassland). The land cover map has a resolution of 10 m and is generated based on Sentinel-2 data applying a deep learning approach. The land cover map mosaic in June and July of 2022 for the Tanzania site and the Colombia site respectively were considered for the land cover classes extraction.

3. Methods

Our methodology encompasses three principal stages, as depicted in Fig. 4:

(1) We first normalized LiDAR point cloud data to produce CHMs. These models facilitated the computation of structural diversity indices, namely Structural Richness (RichnessS), Structural Shannon (ShannonS) Index, and Structural Gini-Simpson (GiniS) Index, which serve as quantifiers of structural diversity.

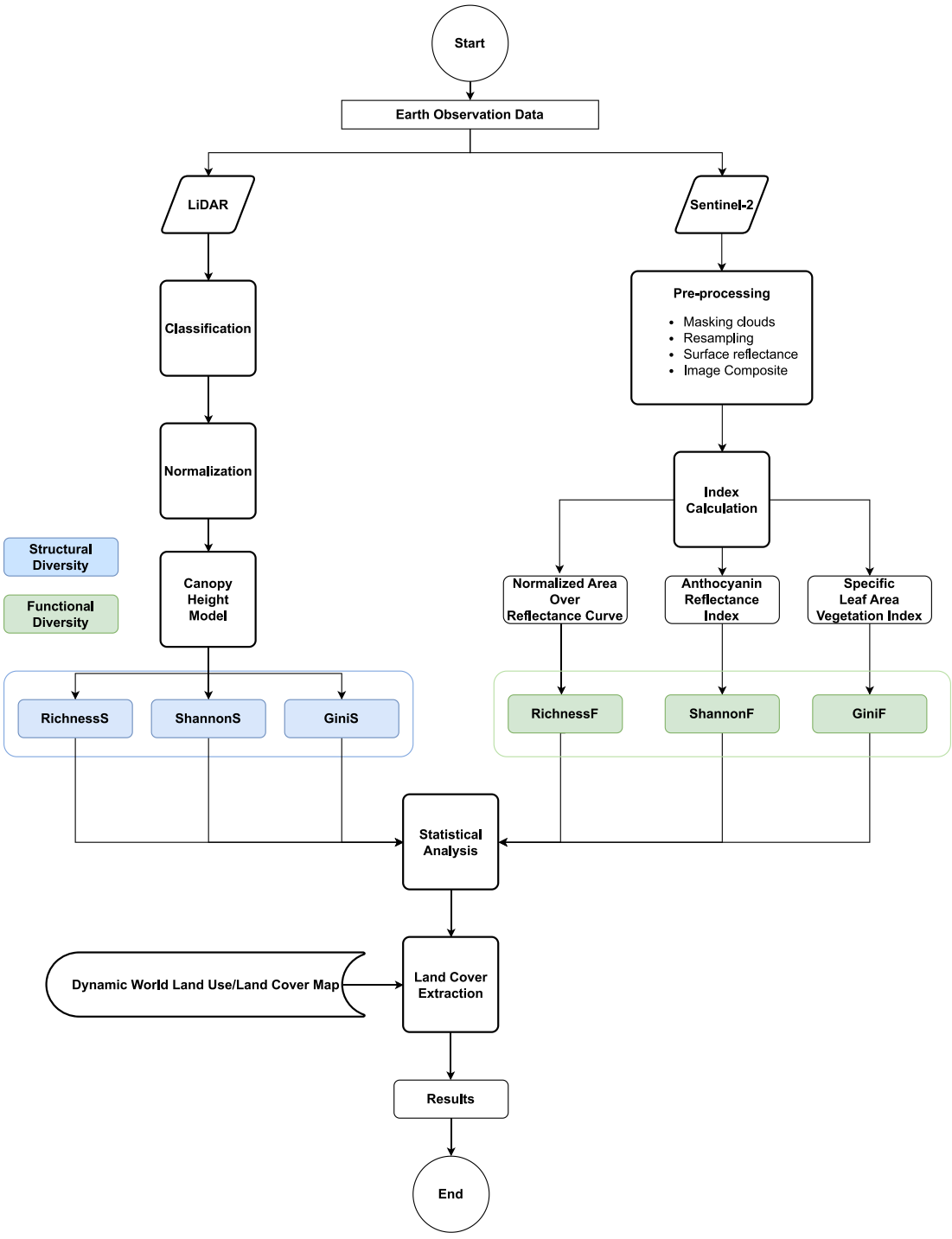

Fig. 4. Overview of the methods used in this study.

(2) Sentinel-2 imagery was preprocessed to yield surface reflectance. Subsequently, we computed three vegetation indices: the Normalized Area Over reflectance Curve (NAOC), Anthocyanin Reflectance Index (ARI), and Specific Leaf Area Vegetation Index (SLAVI). Utilizing these indices, we derived plant functional diversity indices, including Functional Richness (RichnessF), Functional Shannon (ShannonF) Index, and Functional Gini-Simpson (GiniF) Index.

(3) We performed a statistical analysis to investigate the relationship between these two facets of diversity across varying spatial scales and distinct ecoregions.

3.1. Calculation of structural diversity

In order to capture the 3D structural complexity, three distinctive indices, namely ShannonS (Torresani et al., 2020), GiniS (Gasc et al., 2013), and RichnessS were calculated to represent structural diversity. The original Shannon index was developed by Shannon (1948) which focuses on both the richness and evenness component, while the Gini-Simpson index (Simpson, 1949) lays greater emphasis on the evenness component and on the dominant species (Nagendra, 2002). Richness refers to the number of diverse units and evenness to the distribution thereof.

The ShannonS was calculated from LiDAR Data based on the generated CHM (Torresani et al., 2020). The Shannon index, which was originally used for species diversity, is calculated as follows:

$$Shannon = -\sum_{i=1}^{s} p_i \cdot ln(p_i) \tag{1}$$

where s is the total number of species and p_i is the proportion of total sample represented by species i. It ranges from 0 to infinity, estimating the uncertainty in predicting which species a randomly selected individual belongs to. For ShannonS, the species is replaced by the 0.5 m height layers and the p_i indicates the proportion of pixels in the CHM that fall within a specific height category (Listopad et al., 2015).

We also calculated the GiniS (Gasc et al., 2013) based on the LiDAR-derived CHM. The Gini-Simpson index defines the probability of two randomly selected samples belonging to different species. It is calculated as follows:

$$\text{Gini-Simpson} = 1 - \sum_{i=1}^{s} p_i^2 \tag{2}$$

RichnessS was also calculated by counting the number of height layers from the CHM per pixel.

3.2. Functional diversity estimation

Three physiological functional traits, namely leaf chlorophyll content (CHL), leaf anthocyanin content (ANTH) and specific leaf area (SLA) have been selected for functional diversity estimation. These three functional traits were selected based on their ecological importance.

Chlorophyll is the photosynthetic pigment in leaves that absorbs light energy for photosynthesis. It is one of the primary pigments of plant leaves, which provides valuable information of plant productivity status (Croft et al., 2020). CHL is defined as the relative content of chlorophyll a+b per unit leaf area (Palta, 1990). Vegetation chlorophyll content plays a key role in photosynthesis and conversion of solar energy into stored chemical energy (Croft et al., 2015). Moreover, it is a good indicator of plant physiological condition (Croft et al., 2015).

ANTH are pigments found naturally in all the tissues of higher plants (Gitelson et al., 2001). ANTH can be induced by biotic or abiotic stress to help plants cope with the adverse effects of the stress (Li and Huang, 2021). They provide valuable information about the physiological status of plants, as they are considered indicators of various types of plant stresses and plant physiological status (Gitelson et al., 2009).

SLA, the inverse of leaf mass per area (LMA), links biomass and water cycles as well as quantifying plant physiological processes (Ali et al., 2017; Kimball et al., 2002). It is defined as the ratio between leaf area and leaf dry mass, and plays an important role in plant growth modeling (Garnier et al., 2001). SLA can be linked with plant carbon and water cycles, and provides important information on the variation of photosynthetic capacity and leaf nitrogen content (Ali et al., 2016).

3.2.1. Vegetation indices as proxies for functional traits

We selected three proxies for the functional traits based on previous studies. In this regard, NAOC, an index that is derived from hyperspectral data, was adapted for CHL assessment using Sentinel-2 data. NAOC has been proven to act as a reliable predictor of CHL that has a strong correlation with in-situ CHL data (Delegido et al., 2011). It was designed for the estimation of CHL of heterogeneous regions with various crops, canopy and different types of bare soil, which is suitable for our application in agroforestry areas with mixed vegetation (Delegido et al., 2010).

It is given by:

$$NAOC = 1 - \frac{\int_a^b R \cdot d\lambda}{(b-a) \cdot R_b} \tag{3}$$

where λ is the wavelength, R denotes reflectance, R_b is the maximum red edge reflectance, and a and b are the integration limits of the CHL absorption centered at 670 nm. For the calculation for Sentinel-2, a equals 665 nm, and b equals 783 nm.

To compute ANTH from Sentinel-2 data, ARI which was specifically designed to estimate anthocyanin levels in plant leaves was employed. Previous studies have demonstrated a strong correlation between the ARI and ANTH (Hawryło et al., 2018; Merzlyak et al., 2008). It was found that the reflectance at around 700 nm was closely related to CHL, while the reflectance at around 550 nm (green range) was related to both CHL and ANTH (Gitelson et al., 2001). Thus, to calculate ANTH, the following formula was proposed (Gitelson et al., 2001):

$$ARI = \frac{1}{R_{560}} - \frac{1}{R_{704}} \tag{4}$$

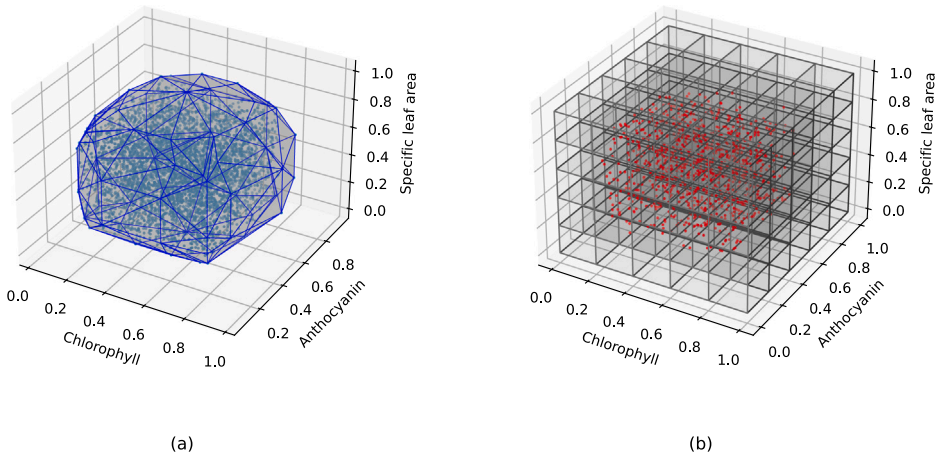

Fig. 5. Visualization of functional diversity calculation: (**a**) Convex hull volume (RichnessF), (**b**) ShannonF.

where R_{560} denotes as the reflectance at 560 nm and R_{704} stands for the reflectance at 704 nm.

Previously, it was shown that SLAVI had a strong correlation with SLA (Lymburner et al., 2000). It was proposed due to the relationship between red, near-infrared and Short-wave infrared reflectance and SLA (Lymburner et al., 2000). SLAVI was computed as follows:

$$SLAVI = \frac{R_{842}}{R_{665} + R_{2190}} \tag{5}$$

where R_{842} is the reflectance at 842 nm, R_{665} is the reflectance at 665 nm, and R_{2190} is the reflectance at 2190 nm.

3.2.2. From vegetation indices to functional diversity indicies

RichnessF, a measure of niche extent, was calculated based on the convex hull volume (CHV), which is a construct from computational geometry (Hauser et al., 2021). It is calculated by constructing a moving window of pixels in the functional space. The 3D axes are defined by the three functional traits. RichnessF was then obtained by estimating the convex hull volume of the moving window pixels. It is sensitive to outliers and anomalies (Schneider et al., 2017). The visualization of the CHV is shown in Fig. 5(a).

To assess both the functional richness and evenness, The Shannon and Gini-Simpson indices were modified (i.e., ShannonF and GiniF) for plant functional diversity assessment. Instead of working with individual species (Eq (1)), the three functional traits are scaled between 0 and 1 with min–max scaling, and binned into 3D voxels where each voxel acts as an individual species (Fig. 5(b)). p_i is then the proportion of the total number of pixels (red dots) that fall within the i^{th} voxel. By binning the functional traits, all pixels are considered for calculating the ShannonF. The Gini-Simpson index was also adapted for the functional biodiversity calculation. In Eq. (2), instead of working with species, p_i indicates the proportion of pixels that fall within a specific voxel to the total number of pixels. The ShannonF and GiniF take into account not only the number of voxels as richness, but also considers the number of pixels within each voxel. They are generally less affected by outliers compared to measures of richness due to their mathematical properties. In Richness measures, each voxel, regardless of how many individuals are present, contribute equally to the total count. Therefore, the addition or loss of one voxel has a direct impact on the count. However, outliers with low abundance contribute very little to ShannonF and GiniF because their proportional abundance is very low (Stirling and Wilsey, 2001). This reduces their impact on the overall diversity calculations.

To calculate the functional diversity using Sentinel-2 indices, we used a moving window approach with three different window sizes (i.e., 3 × 3, 5 × 5 and 10 × 10). The results have been compared with the reference data, the LiDAR-generated structural indices.

3.3. Statistical analysis

To compare the performance of different indicators, Pearson correlation coefficient (r) and P value were applied for testing non-correlation (Pearson, 1896). The Pearson correlation coefficient r is calculated as follows:

$$r = \frac{\sum_{i=1}^{n}(X_i - \overline{X})(Y_i - \overline{Y})}{\sqrt{\sum_{i=1}^{n}(X_i - \overline{X})^2}\sqrt{\sum_{i=1}^{n}(Y_i - \overline{Y})^2}} \tag{6}$$

where r represents the degree of linear correlation between two variables X and Y. X_i is the value of variable X for the i^{th} observation, and Y_i is the value of variable Y for the i^{th} observation. $\bar{X}$ and $\bar{Y}$ are the means of the variables X and Y respectively.

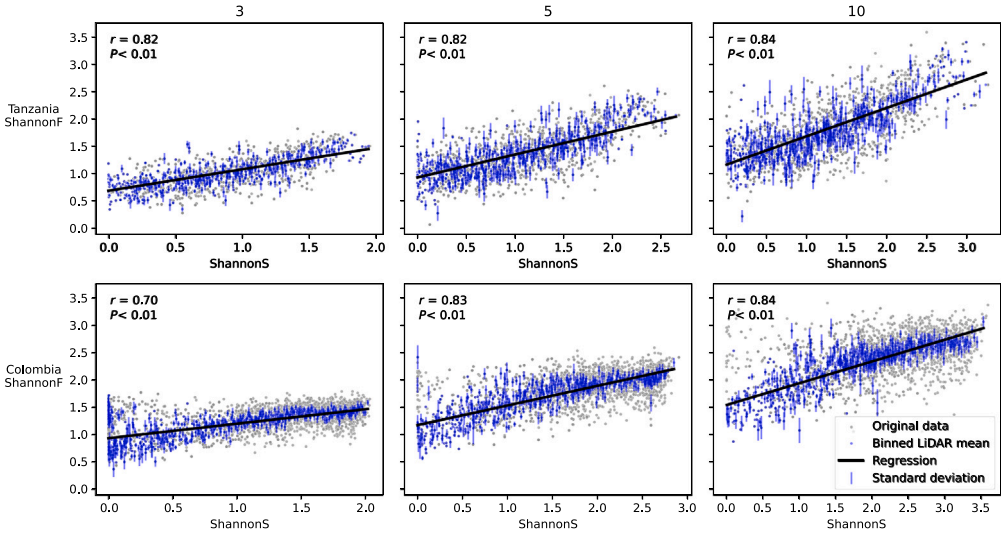

Fig. 6. Comparison between structural diversity (ShannonS) and functional diversity (ShannonF) in different sites.

Table 1
Mean value of functional diversity and structural diversity at different scales (scaled).

Window size	RichnessF	ShannonF	GiniF	RichnessS	ShannonS	GiniS
3	1	1	1	1	1	1
5	5.81	1.37	1.18	1.88	1.34	1
10	28.34	1.81	1.35	3.67	1.60	1

4. Results

4.1. Scale effects on biodiversity

The comparison between structural diversity and functional diversity based on different scales (i.e., window sizes) is illustrated in Fig. 6. The most notable correlation between ShannonF and ShannonS was observed when using a window size of 10 × 10 in both sites (r = 0.84 for Tanzania and Colombia), whereas the difference between a window size of 10 × 10 and 5 × 5 was not deemed significant (Fig. 6). Notably, the correlation between ShannonF and ShannonS was markedly lower when employing a window size of 3 × 3 in the Colombia site (r = 0.70). It should be highlighted that there was no difference observed between the correlation between ShannonF and ShannonS using a window size of 5 × 5 and 3 × 3 for the Tanzania site.

Fig. 7 shows the change in biodiversity across various scales (i.e., window sizes). It is observed that both structural and functional diversity increased as the scales expanded in both sites. The increase of structural and functional diversity was most pronounced for the richness measures, followed by the Shannon indices, while the Gini indices were least affected by the change of scales. In particular, the GiniS was independent of scales. Additionally, functional diversity exhibited a higher average value compared to structural diversity in both sites (Fig. 7).

Comparing the study sites, the Colombia site exhibited a greater level of functional and structural biodiversity than the Tanzanian site. The scaled mean values of functional diversity and structural diversity, combined for both sites at different scales, are presented in Table 1, where each variable based on window size 3 was converted to 1. Other variables have been scaled relative to window size 3 using their transformation. As indicated by the indices, functional diversity exhibited a considerably more pronounced increase than structural diversity for all variables. RichnessF demonstrated the most significant increase from window size 3 to 10 (28 times), while the GiniF index had the smallest increase (1.35 times). Structural diversity showed a similar but less pronounced trend, with no discernible change in GiniS.

4.2. Comparison between different indicators

Significant correlations (r) were observed between many of the structural and functional diversity variables for both sites (Fig. 8). Notably, there was a high correlation between functional richness (RichnessR) and structural richness (RichnessS) (r = 0.81 in Tanzania, r = 0.76 in Colombia). Additionally, ShannonF and ShannonS, exhibited a strong correlation with an r of 0.84 in both sites. However, the correlation between GiniF and GiniS was less consistent, with a stronger correlation observed in Colombia (r = 0.82) compared to Tanzania (r = 0.67).

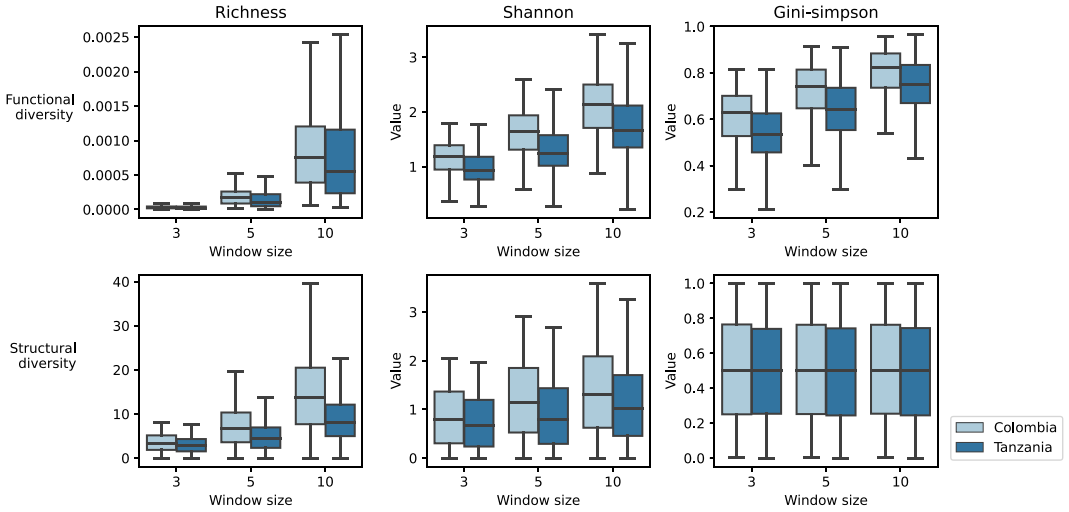

Fig. 7. Boxplots of functional diversity and structural diversity at different scales.

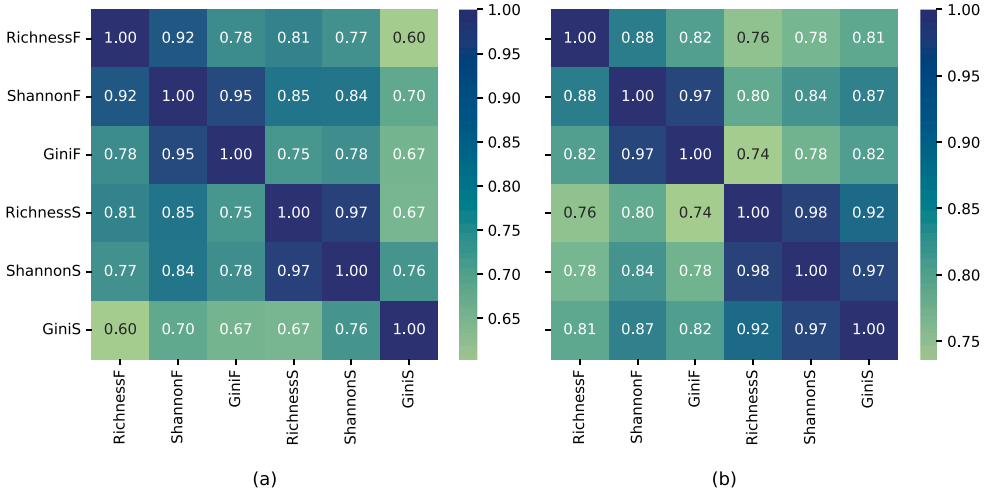

Fig. 8. Cross-correlation matrix of biodiversity variables in two study sites: (**a**) Tanzania, (**b**) Colombia.

4.3. Mapping of functional biodiversity in different ecoregions

To compare the differences in biodiversity in different ecoregions and land cover types, Fig. 9 illustrates the average values of ShannonF and ShannonS extracted from the land cover maps for three land cover classes (i.e., trees, grassland, cropland). Both sites consistently displayed similar trends in terms of structural and functional diversity. Tree land cover were found to be more diverse in terms of both structural and functional diversity in both sites. Cropland showed comparable levels of functional and structural diversity to grassland in the Colombia site, and a higher diversity than grassland in the Tanzania site.

Fig. 10 shows a distribution of the three vegetation indices and Shannon index derived from LiDAR (ShannonS) for our two study sites. The diversity had a different distribution for the two sites, with Colombia being skewed towards higher values for NAOC, SLAVI and ShannonS, while the difference of ARI is not significant.

Furthermore, Figs. 11 and 12 provides a visual interpretation of the functional diversity (ShannonF) map for the Colombia site and the Tanzania site, highlighting that trees exhibit a higher functional diversity level compared to grassland and cropland.

5. Discussion

In this study, we aimed to enhance the quality of functional diversity mapping using Sentinel-2 data by modifying the species Shannon index for plant functional traits in a 3D space based on the proxies (vegetation indices) of three important traits including CHL, ANTH, and SLA. Airborne LiDAR data were utilized to assess the mapped functional richness and evenness. Our results

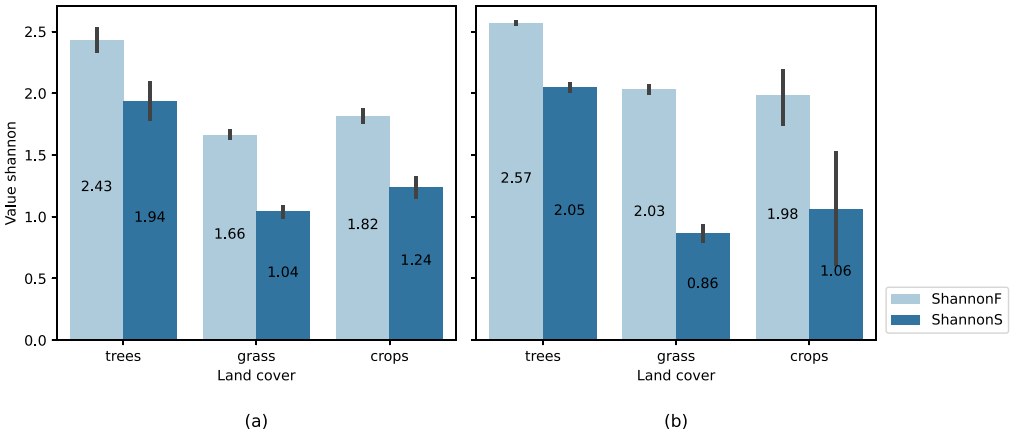

Fig. 9. Bar plots of mean ShannonF and ShannonS for three different land cover types, including trees, cropland and grassland in two study sites: (**a**) Tanzania, (**b**) Colombia. (Vertical black lines indicate the standard deviation.)

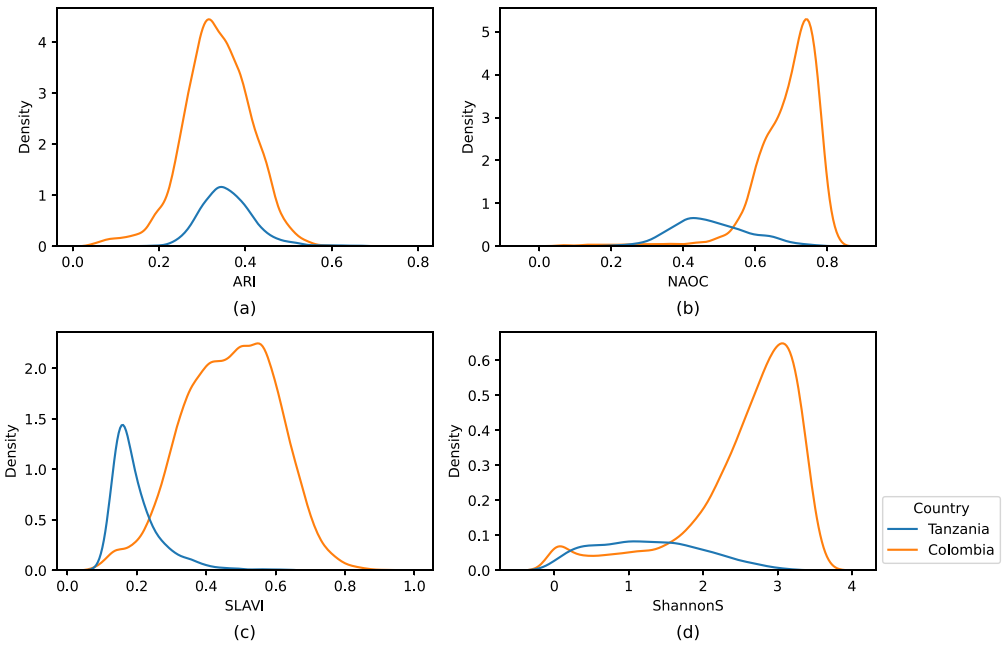

Fig. 10. Distribution of vegetation indices and ShannonS for two study sites: (**a**) ARI, (**b**) NAOC, (**b**) SLAVI, (**b**) ShannonS.

demonstrated that there is a significant correlation between plant functional and structural diversity when measured with Shannon and Gini-Simpson index at different scales. Specifically, the proposed functional diversity index ShannonF had the strongest correlation with LiDAR-derived structural biodiversity variables.

In order to evaluate the scale effects on functional and structural diversity, diversity variables were calculated with different moving window sizes. The window size is a common parameter for spectral biodiversity measurement with a larger window size covering a broader area. In both sites, the agreement between functional diversity and structural diversity variables showed a stronger correlation at the large scale using a window size of 10 × 10 (100 m) (Fig. 6). This could be partially attributed to the fact that at a larger scale, the noise of the signals as well as the geometric misalignment between Sentinel-2 and LiDAR were minimized (Saatchi et al., 2011). Moreover, a larger diversity variation was also observed at a larger scale which might be better captured by both sensors (i.e., LiDAR and Sentinel-2) than a small variation. At a larger scale, it is more likely to have different vegetation types as well as vegetation height, resulting in a stronger agreement between functional and structural diversity. This is also the reason why both diversity variables increased as moving window size increased (Fig. 7). However, the increase in both functional and structural biodiversity variables with the scale was much less significant for the Gini-Simpson index than for richness and Shannon diversity (Table 1). Shannon index and Gini-Simpson index both consider richness and evenness, whereas Shannon index focuses more on the richness component, and the Gini-Simpson index focuses on the evenness component and on the dominant

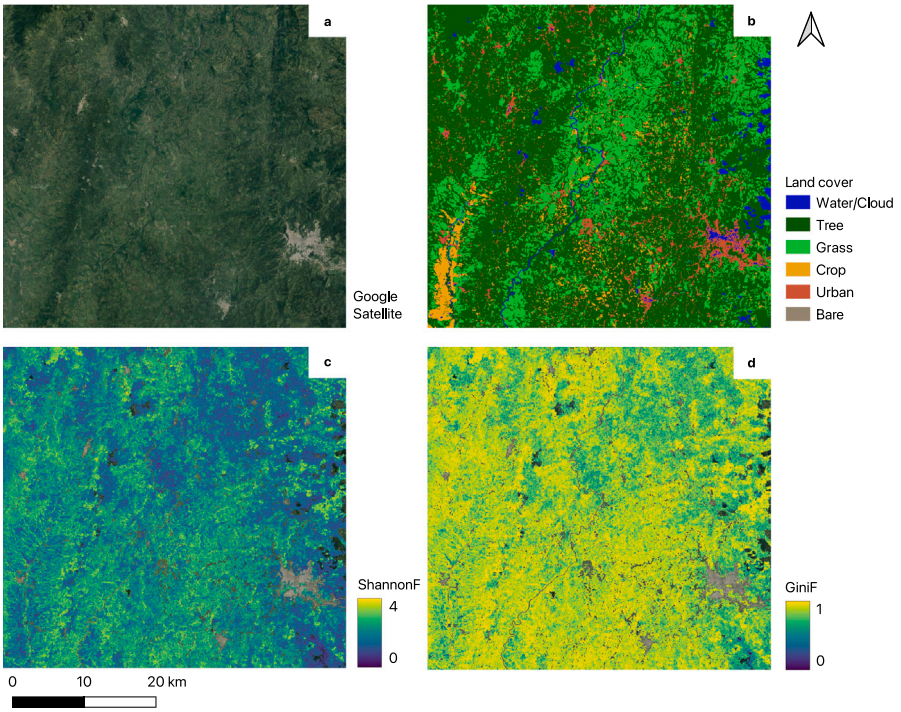

Fig. 11. Large area functional diversity mapping in the Colombia site: (**a**) Google satellite RGB basemap, (**b**) Land cover map, (**c**) ShannonF mapping, (**d**) GiniF mapping.

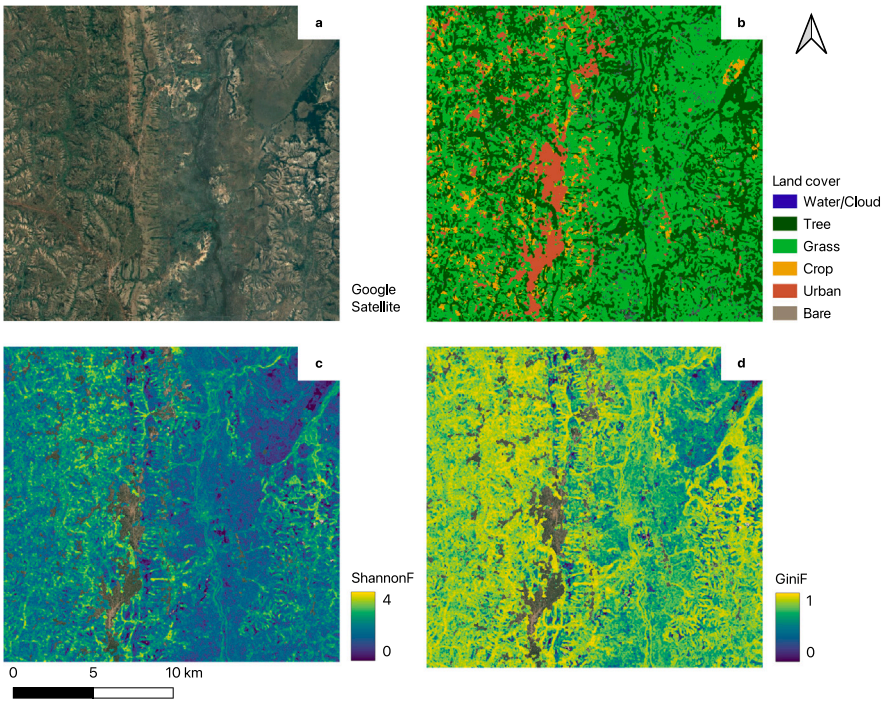

Fig. 12. Large area functional diversity mapping in the Tanzania site: (**a**) Google satellite RGB basemap, (**b**) Land cover map, (**c**) ShannonF mapping, (**d**) GiniF mapping.

species (Nagendra, 2002). It indicates that as the spatial scale increases, richness increases much more significantly than evenness. A previous study by Schneider et al. (2017) showed that functional evenness is much less dependent on the study scale than richness. Our findings are in agreement with Schneider et al. (2017) as we have also observed that the increase was less drastic for the structural diversity variables than the functional diversity variables (Fig. 7). Specifically, the GiniS is much less affected by scale. One of the key differences between the two types of biodiversity variables in this study was that the functional diversity considered three different traits (i.e., CHL, ANTH and SLA), while the structural diversity only included height. These three traits reflect different physiological status of plants. More traits are more likely to capture and highlight the subtle differences between different plants, since plants exhibit their variation in different aspects. Height, as a single structural trait, might capture less variation than the other three functional traits. Therefore, it is reasonable that the richness component had a more significant increase for the functional traits than the structural traits, which contributed to the larger increase in both Shannon and Gini-Simpson indices.

We have observed significant correlations between the three functional diversity variables and three structural diversity variables in both regions (Fig. 8), while the correlation varied among these variables. As expected, the cross-correlation within the diversity variables was strong which is expected, since Shannon and Gini-Simpson indices both have the richness component. Across all diversity variables, LiDAR-derived structural diversity exhibited lower values than the functional diversity derived from Sentinel-2 data. Specifically, at the low range of the diversity, ShannonS showed a much lower variation than the ShannonF (Fig. 6). When only low grass is found in the area, the height has a very low variation, leading to a low ShannonS. However, the spectral variation based on the functional traits between different grass species and within the species could still be captured by Sentinel-2 data, especially in the red edge and near-infrared domain, showing differences in leaf biochemical content. Another factor is that it is more challenging for LiDAR ground classification in low vegetation areas, as low vegetation can confound ground classification algorithms, and be misclassified as ground (Moudrý et al., 2020). Applying normalization on low vegetation might lead to zero height in this situation. An alternative approach would involve foregoing height normalization in estimating structure diversity. However, this is beyond conjecture and requires additional research and investigation.

Our finding revealed a stronger correlation between the ShannonF and three structural diversity variables compared to the RichnessF and the GiniF (Fig. 8), demonstrating the effectiveness of this proposed variable for biodiversity mapping. It takes into account both richness and evenness. The method can be potentially scaled up to higher dimensions considering more plant functional traits such as leaf water content and leaf area index. We applied three vegetation indices (i.e., NAOC, ARI and SLAVI) as proxies to estimate plant traits (Helfenstein et al., 2022). It is demonstrated that NAOC as a proxy for leaf CHL content was significantly higher in the Colombia site than in the Tanzania site (Fig. 11), which is an indication of higher productivity in the Colombia site (Peng and Gitelson, 2012). A similar trend has been observed for SLAVI (Fig. 11). Usually, high SLA occurs in areas with high water and nutrient availability (Long et al., 2011), which is in agreement with our observation. Sentinel-2 data provide multiple bands in the near-infrared and red-edge region making it feasible for the retrieval of certain plants traits, while traits like leaf carotenoid content are more difficult to estimate with Sentinel-2 data. It requires narrow band indices including the wavelength around 510 nm (Gitelson et al., 2002) which is unavailable for Sentinel-2. Therefore, leaf anthocyanin content was chosen instead. However, anthocyanins are induced in plants in response to abiotic stresses such as drought. This limited our study period to the dry season when the concentrations of anthocyanin were higher (Cheng et al., 2014). Therefore, applying narrow-band hyperspectral data enables the measurement of various plant traits, including carotenoid content, without restricting the time period for measurement.

The differences between functional diversity and structural diversity could be partially attributed to the image capturing dates. There were 3–4 months differences in the Sentinel-2 capturing data and the airborne LiDAR capturing date. Ideally it is advised to coincide the image dates for the two types of data for the comparison within the same period. The main reason to choose June and July for Sentinel-2 data was to obtain the imagery in the dry season to avoid cloud cover, which was quite a challenge in the tropical region. That being said, LiDAR was mainly used to capture the structural information, which was not affected by the dry and wet seasons. Additionally, the growth in height in the dry season was minimal. Thus, we did not expect much change in terms of canopy height during the 3–4 months. Therefore, it is reasonable to assume that the canopy height in June and July can be associated with the imagery captured by Sentinel-2. However, another aspect is that the management practices can also affect the biodiversity calculation since the study areas are mainly agroforestry systems. To tackle this problem, either radar data which are not affected by cloud should be considered, or LiDAR data need to be obtained in the same period with Sentinel-2 data. It is also worth noting that the images should always come from the same period (dry season) for the change detection for different years.

Our functional and structural mapping across the three land cover classes — tree cover, grassland and cropland, in the two different study areas confirmed our assumption that trees support greater biodiversity than grassland and cropland (Fig. 9). For the tree cover class, a higher functional and structural biodiversity was observed in the Colombia site than in the Tanzania site (Fig. 9). This can be due to the fact that the Colombia site is in the tropical and subtropical moist broadleaf forests region, while the Tanzania site is located in the tropical and subtropical grasslands, savannas, and shrublands region, and the tree species are more diverse (Brun et al., 2019), exhibiting higher variation in plant functional traits and height. Regarding the grassland and cropland, the Colombia site also showed a higher diversity in terms of functional diversity, while the structural diversity did not show a significant difference, as it is less sensitive to low vegetation. The higher functional diversity of these two land cover types in Colombia could be attributed to the climate conditions (Hu et al., 2022). In the Colombia site, the rainfall was much higher, and the links between high rainfall and rich biodiversity are well-established (Hu et al., 2022). Although no significant difference was observed regarding the mean value for the structural diversity, the standard deviation (Fig. 9) was much higher in the Colombia site, especially for the cropland class. This could be caused by certain mixed pixels of trees and cropland/grassland due to the 10 m resolution of the Sentinel-2 data. When trees are included in a pixel, the diversity becomes much higher. Another possible reason could be that in the Colombia site, often bigger trees are planted to implement agroforestry, which provides shade for crops like

coffee (Bosselmann et al., 2009; De Leijster et al., 2021). It suggests that agroforestry systems may have an impact on functional and structural biodiversity. Thoughtful implementation and consideration of local context can potentially enhance their positive impact on our natural environment.

It is important to note that this study is subject to a few limitations worth discussing. Specifically, in situ data collection was not conducted for this research in order to estimate functional diversity. Consequently, vegetation indices were applied as proxies for functional traits. While we were cautious and selective in choosing the indices, this approach may introduce a degree of inaccuracy. For instance, SLAVI has been considered as a relatively new index for estimating SLA (Kim et al., 2024) using Earth observation data. Therefore, more investigation needs to be done in order to fully understand the relationship between SLAVI as a proxy of SLA, and the extent to which plant functional traits influence SLAVI. In addition, while the ARI was broadly applied as a proxy of ANTH, the effectiveness of ARI may vary across. However, the ARI has been widely applied as a proxy for ANTH its efficacy may fluctuate among various plant species owing to disparities in anthocyanin accumulation patterns and spectral responses. Moreover, when applying Earth observation data to derive vegetation indices, it is significant to recognize the impact of various environmental elements like soil composition as a background, atmospheric conditions, and the structure of the canopy. These factors have the potential to introduce inaccuracies in the estimation of these indices.

Our findings suggest that the novel indices ShannonF and GiniF can effectively capture the functional diversity in agroforestry areas. By estimating functional diversity in agroforestry, managers can optimize a range of ecosystem services. Diverse functions help create a more balanced and self-sustaining ecosystems, reducing the need for external inputs like fertilizers and pesticides. Systems with higher functional diversity are generally more resilient to biotic and abiotic stresses, such as drought and diseases as the presence of functionally diverse species provides a more stable ecosystem. Functional diversity also allows different species to efficiently exploit different niches, minimizing competition and maximizing the use of available resources, which help managers optimize the agroforestry system design. Managing for functional diversity often involves choosing species combinations that complement each other's functions and managing the system in a way that maintains and enhances these functions over time.

6. Conclusions

This research focuses on the field of biodiversity monitoring by leveraging advanced remote sensing technologies, including Sentinel-2 satellite imagery and airborne LiDAR data, to evaluate functional and structural diversity in agroforestry areas within two distinct ecoregions. Our study contributes to the understanding of biodiversity on a large scale, offering a novel approach for mapping and comparing different forms of biodiversity. The key findings of our research demonstrate a substantial correlation between functional and structural diversity, particularly at larger spatial scales. This correlation highlights the interdependence of different biodiversity aspects and their collective impact on ecosystem health and functionality.

Moreover, our study reveals that tree land cover class supports greater biodiversity compared to grassland and cropland in both the Victoria Basin forest-savanna mosaic in Tanzania and the Cauca Valley Montane forests in Colombia, with the latter exhibiting particularly high biodiversity levels. These findings have important implications for conservation strategies, as they provide a clearer picture of biodiversity distribution and the relative importance of different land cover types in maintaining ecosystem diversity.

The integration of multiple remote sensing techniques and the development of novel functional diversity indices ShannonF and GiniF in this study represent a significant advancement in ecological monitoring and analysis. Future research could build upon these findings to explore the application of these methods in other ecosystems and to refine the techniques for even more precise biodiversity monitoring.

CRediT authorship contribution statement

Xi Zhu: Writing – review & editing, Writing – original draft, Visualization, Validation, Resources, Methodology, Investigation, Formal analysis, Data curation, Conceptualization. **Mila Luleva:** Writing – review & editing, Methodology, Investigation. **Sebastian Paolini van Helfteren:** Writing – review & editing, Writing – original draft, Investigation, Conceptualization. **Yaqing Gou:** Writing – review & editing, Visualization, Investigation. **Weronika Gajda:** Writing – review & editing, Investigation. **Elnaz Neinavaz:** Writing – review & editing, Visualization, Investigation.

Declaration of competing interest

The authors declare that they have no known competing financial interests or personal relationships that could have appeared to influence the work reported in this paper.

Data availability

The authors do not have permission to share data.

Declaration of Generative AI and AI-assisted technologies in the writing process

During the preparation of this work the authors used ChatGPT in order to improve the readability of the language. After using this tool, the authors reviewed and edited the content as needed and take full responsibility for the content of the publication.

Acknowledgments

We express our heartfelt gratitude to Jelmer van de Mortel for his support for this study. Special thanks are due to Kyle Nielsen, Laura Wools and Dave Verkaik for all their efforts in data collection in Tanzania and Colombia. Without them, this study would not have been possible. Last but not least, we would also like to thank the Acorn team for sharing their rich, local ecological knowledge, contributing significantly to our understanding of the study areas.

References

Ali, A.M., Darvishzadeh, R., Skidmore, A.K., van Duren, I., 2017. Specific leaf area estimation from leaf and canopy reflectance through optimization and validation of vegetation indices. Agricult. Forest Meteorol. 236, 162–174.

Ali, A.M., Darvishzadeh, R., Skidmore, A.K., van Duren, I., Heiden, U., Heurich, M., 2016. Estimating leaf functional traits by inversion of PROSPECT: Assessing leaf dry matter content and specific leaf area in mixed mountainous forest. Int. J. Appl. Earth Obs. Geoinformation 45, 66–76.

Bosselmann, A.S., Dons, K., Oberthur, T., Olsen, C.S., Ræbild, A., Usma, H., 2009. The influence of shade trees on coffee quality in small holder coffee agroforestry systems in Southern Colombia. Agricult. Ecosyst. Environ. 129 (1–3), 253–260.

van Breugel, P., Kindt, R., Lillesø, J.P.B., Bingham, M., Demissew, S., Dudley, C., Friis, I., Gachathi, F., Kalema, J., Mbago, F., et al., 2015. Potential natural vegetation map of eastern africa (burundi, ethiopia, Kenya, malawi, rwanda, tanzania, uganda and zambia). Version 2.0. In: Forest & Landscape Denmark and World Agroforestry Centre. ICRAF, uuurl: http://vegetationmap4africa.org.

Brown, C.F., Brumby, S.P., Guzder-Williams, B., Birch, T., Hyde, S.B., Mazzariello, J., Czerwinski, W., Pasquarella, V.J., Haertel, R., Ilyushchenko, S., Schwehr, K., Weisse, M., Stolle, F., Hanson, C., Guinan, O., Moore, R., Tait, A.M., 2022. Dynamic world, near real-time global 10 m land use land cover mapping. Sci. Data 9 (1).

Brun, P., Zimmermann, N.E., Graham, C.H., Lavergne, S., Pellissier, L., Münkemüller, T., Thuiller, W., 2019. The productivity-biodiversity relationship varies across diversity dimensions. Nature Commun. 10 (1), 5691.

Burgess, N., Hales, J., Underwood, E., Dinerstein, E., Olson, D., Itoua, I., Schipper, J., Ricketts, T., Newman, K., et al., 2004. Terrestrial Ecoregions of Africa and Madagascar: A Conservation Assessment. Island Press.

Butler, H., Chambers, B., Hartzell, P., Glennie, C., 2021. PDAL: An open source library for the processing and analysis of point clouds. Comput. Geosci. 148, 104680.

Cardinale, B.J., Duffy, J.E., Gonzalez, A., Hooper, D.U., Perrings, C., Venail, P., Narwani, A., Mace, G.M., Tilman, D., Wardle, D.A., Kinzig, A.P., Daily, G.C., Loreau, M., Grace, J.B., Larigauderie, A., Srivastava, D.S., Naeem, S., 2012. Biodiversity loss and its impact on humanity. Nature 486 (7401), 59–67.

Cheng, G., He, Y.N., Yue, T.X., Wang, J., Zhang, Z.W., 2014. Effects of climatic conditions and soil properties on cabernet sauvignon berry growth and anthocyanin profiles. Molecules 19 (9), 13683–13703.

Croft, H., Chen, J., Wang, R., Mo, G., Luo, S., Luo, X., He, L., Gonsamo, A., Arabian, J., Zhang, Y., Simic-Milas, A., Noland, T., He, Y., Homolová, L., Malenovský, Z., Yi, Q., Beringer, J., Amiri, R., Hutley, L., Arellano, P., Stahl, C., Bonal, D., 2020. The global distribution of leaf chlorophyll content. Remote Sens. Environ. 236, 111479.

Croft, H., Chen, J., Zhang, Y., Simic, A., Noland, T., Nesbitt, N., Arabian, J., 2015. Evaluating leaf chlorophyll content prediction from multispectral remote sensing data within a physically-based modelling framework. ISPRS J. Photogramm. Remote Sens. 102, 85–95.

De Leijster, V., Santos, M., Wassen, M., Camargo García, J., Llorca Fernandez, I., Verkuil, L., Scheper, A., Steenhuis, M., Verweij, P., 2021. Ecosystem services trajectories in coffee agroforestry in Colombia over 40 years. Ecosyst. Serv. 48, 101246.

Delegido, J., Alonso, L., Gonzalez, G., Moreno, J., 2010. Estimating chlorophyll content of crops from hyperspectral data using a normalized area over reflectance curve (NAOC). Int. J. Appl. Earth Obs. Geoinf. 12 (3), 165–174.

Delegido, J., Verrelst, J., Alonso, L., Moreno, J., 2011. Evaluation of sentinel-2 red-edge bands for empirical estimation of green LAI and chlorophyll content. Sensors 11 (7), 7063–7081.

Drusch, M., Del Bello, U., Carlier, S., Colin, O., Fernandez, V., Gascon, F., Hoersch, B., Isola, C., Laberinti, P., Martimort, P., et al., 2012. Sentinel-2: ESA's optical high-resolution mission for GMES operational services. Remote Sens. Environ. 120, 25–36.

Félix, G.F., Diedhiou, I., Le Garff, M., Timmermann, C., Clermont-Dauphin, C., Cournac, L., Groot, J.C., Tittonell, P., 2018. Use and management of biodiversity by smallholder farmers in semi-arid West Africa. Global Food Secur. 18, 76–85.

Garnier, E., Shipley, B., Roumet, C., Laurent, G., 2001. A standardized protocol for the determination of specific leaf area and leaf dry matter content. Functional Ecol. 688–695.

Gasc, A., Sueur, J., Jiguet, F., Devictor, V., Grandcolas, P., Burrow, C., Depraetere, M., Pavoine, S., 2013. Assessing biodiversity with sound: Do acoustic diversity indices reflect phylogenetic and functional diversities of bird communities? Ecol. Indic. 25, 279–287.

Gitelson, A.A., Chivkunova, O.B., Merzlyak, M.N., 2009. Nondestructive estimation of anthocyanins and chlorophylls in anthocyanic leaves. Am. J. Bot. 96 (10), 1861–1868.

Gitelson, A.A., Merzlyak, M.N., Chivkunova, O.B., 2001. Optical properties and nondestructive estimation of anthocyanin content in plant leaves. Photochem. Photobiol. 74 (1), 38–45.

Gitelson, A.A., Zur, Y., Chivkunova, O.B., Merzlyak, M.N., 2002. Assessing carotenoid content in plant leaves with reflectance spectroscopy. Photochem. Photobiol. 75 (3), 272.

Hamilton, A.J., 2005. Species diversity or biodiversity? J. Environ. Manage. 75 (1), 89–92.

Hauser, L.T., Féret, J.B., An Binh, N., van der Windt, N., Sil, A.F., Timmermans, J., Soudzilovskaia, N.A., van Bodegom, P.M., 2021. Towards scalable estimation of plant functional diversity from sentinel-2: In-situ validation in a heterogeneous (semi-)natural landscape. Remote Sens. Environ. 262, 112505.

Hawryło, P., Bednarz, B., Wężyk, P., Szostak, M., 2018. Estimating defoliation of scots pine stands using machine learning methods and vegetation indices of sentinel-2. Eur. J. Remote Sens. 51 (1), 194–204.

Helfenstein, I.S., Schneider, F.D., Schaepman, M.E., Morsdorf, F., 2022. Assessing biodiversity from space: Impact of spatial and spectral resolution on trait-based functional diversity. Remote Sens. Environ. 275, 113024.

Hu, Y., Li, X., Guo, A., Yue, P., Guo, X., Lv, P., Zhao, S., Zuo, X., 2022. Species diversity is a strong predictor of ecosystem multifunctionality under altered precipitation in desert steppes. Ecol. Indic. 137, 108762.

Ilangakoon, N., Glenn, N.F., Schneider, F.D., Dashti, H., Hancock, S., Spaete, L., Goulden, T., 2021. Airborne and spaceborne lidar reveal trends and patterns of functional diversity in a semi-arid ecosystem. Front. Remote Sens. 2, 743320.

Kattan, G., 2018. Northern South America: Central Colombia. World Wildlife Fund, URL https://www.worldwildlife.org/ecoregions/nt0109. (Accessed 22 February 2024).

Kim, J., Khouakhi, A., Corstanje, R., Johnston, A.S., 2024. Greater local cooling effects of trees across globally distributed urban green spaces. Sci. Total Environ. 911, 168494.

Kimball, B., Kobayashi, K., Bindi, M., 2002. Responses of agricultural crops to free-air CO2 enrichment. Adv. Agron. 77, 293–368.

LaRue, E.A., Knott, J.A., Domke, G.M., Chen, H.Y., Guo, Q., Hisano, M., Oswalt, C., Oswalt, S., Kong, N., Potter, K.M., Fei, S., 2023. Structural diversity as a reliable and novel predictor for ecosystem productivity. Front. Ecol. Environ. 21 (1), 33–39.
Laurila-Pant, M., Lehikoinen, A., Uusitalo, L., Venesjärvi, R., 2015. How to value biodiversity in environmental management? Ecol. Indic. 55, 1–11.
Li, Y., Huang, J., 2021. Leaf anthocyanin content retrieval with partial least squares and gaussian process regression from spectral reflectance data. Sensors 21 (9), 3078.
Listopad, C.M., Masters, R.E., Drake, J., Weishampel, J., Branquinho, C., 2015. Structural diversity indices based on airborne LiDAR as ecological indicators for managing highly dynamic landscapes. Ecol. Indic. 57, 268–279.
Liu, X., Frey, J., Munteanu, C., Still, N., Koch, B., 2023. Mapping tree species diversity in temperate montane forests using sentinel-1 and sentinel-2 imagery and topography data. Remote Sens. Environ. 292, 113576.
Long, W., Zang, R., Schamp, B.S., Ding, Y., 2011. Within-and among-species variation in specific leaf area drive community assembly in a tropical cloud forest. Oecologia 167, 1103–1113.
Lymburner, L., Beggs, P.J., Jacobson, C.R., et al., 2000. Estimation of canopy-average surface-specific leaf area using landsat TM data. Photogramm. Eng. Remote Sens. 66 (2), 183–192.
Ma, M., 2005. Species richness vs evenness: independent relationship and different responses to edaphic factors. Oikos 111 (1), 192–198.
Ma, X., Mahecha, M.D., Migliavacca, M., van der Plas, F., Benavides, R., Ratcliffe, S., Kattge, J., Richter, R., Musavi, T., Baeten, L., et al., 2019. Inferring plant functional diversity from space: the potential of sentinel-2. Remote Sens. Environ. 233, 111368.
Main-Knorn, M., Pflug, B., Louis, J., Debaecker, V., Müller-Wilm, U., Gascon, F., 2017. Sen2Cor for sentinel-2. In: Image and Signal Processing for Remote Sensing XXIII, vol. 10427, SPIE, pp. 37–48.
Makino, Y., Geringer, M., Manuelli, S., 2020. Promoting mountain biodiversity through sustainable value chains. Mt. Res. Dev. 40 (4).
Merzlyak, M.N., Chivkunova, O.B., Solovchenko, A.E., Naqvi, K.R., 2008. Light absorption by anthocyanins in juvenile, stressed, and senescing leaves. J. Exp. Bot. 59 (14), 3903–3911.
Moudrý, V., Klápště, P., Fogl, M., Gdulová, K., Barták, V., Urban, R., 2020. Assessment of LiDAR ground filtering algorithms for determining ground surface of non-natural terrain overgrown with forest and steppe vegetation. Measurement 150, 107047.
Mura, M., McRoberts, R.E., Chirici, G., Marchetti, M., 2015. Estimating and mapping forest structural diversity using airborne laser scanning data. Remote Sens. Environ. 170, 133–142.
Nagendra, H., 2002. Opposite trends in response for the Shannon and simpson indices of landscape diversity. Appl. Geogr. 22 (2), 175–186.
Olson, D.M., Dinerstein, E., Wikramanayake, E.D., Burgess, N.D., Powell, G.V., Underwood, E.C., D'amico, J.A., Itoua, I., Strand, H.E., Morrison, J.C., et al., 2001. Terrestrial ecoregions of the world: A new map of life on earth: A new global map of terrestrial ecoregions provides an innovative tool for conserving biodiversity. BioScience 51 (11), 933–938.
Palmroos, I., Norros, V., Keski-Saari, S., Mäyrä, J., Tanhuanpää, T., Kivinen, S., Pykälä, J., Kullberg, P., Kumpula, T., Vihervaara, P., 2023. Remote sensing in mapping biodiversity–A case study of epiphytic lichen communities. Forest Ecol. Manag. 538, 120993.
Palta, J.P., 1990. Leaf chlorophyll content. Remote Sens. Rev. 5 (1), 207–213.
Pantera, A., Mosquera-Losada, M., Herzog, F., Den Herder, M., 2021. Agroforestry and the environment. Agrofor. Syst. 95 (5), 767–774.
Pearson, K., 1896. VII. Mathematical contributions to the theory of evolution.—III. Regression, heredity, and panmixia. Philos. Trans. R. Soc. Lond. Ser. A Contain. Pap. Math. Phys. Charact. (187), 253–318.
Peng, Y., Gitelson, A.A., 2012. Remote estimation of gross primary productivity in soybean and maize based on total crop chlorophyll content. Remote Sens. Environ. 117, 440–448.
Rands, M.R.W., Adams, W.M., Bennun, L., Butchart, S.H.M., Clements, A., Coomes, D., Entwistle, A., Hodge, I., Kapos, V., Scharlemann, J.P.W., Sutherland, W.J., Vira, B., 2010. Biodiversity conservation: Challenges beyond 2010. Science 329 (5997), 1298–1303.
Richter, R., Wang, X., Bachmann, M., Schläpfer, D., 2011. Correction of cirrus effects in sentinel-2 type of imagery. Int. J. Remote Sens. 32 (10), 2931–2941.
Rocchini, D., Bacaro, G., Chirici, G., Da Re, D., Feilhauer, H., Foody, G.M., Galluzzi, M., Garzon-Lopez, C.X., Gillespie, T.W., He, K.S., et al., 2018. Remotely sensed spatial heterogeneity as an exploratory tool for taxonomic and functional diversity study. Ecol. Indic. 85, 983–990.
Saatchi, S., Marlier, M., Chazdon, R.L., Clark, D.B., Russell, A.E., 2011. Impact of spatial variability of tropical forest structure on radar estimation of aboveground biomass. Remote Sens. Environ. 115 (11), 2836–2849.
Schneider, F.D., Longo, M., Paul-Limoges, E., Scholl, V.M., Schmid, B., Morsdorf, F., Pavlick, R.P., Schimel, D.S., Schaepman, M.E., Moorcroft, P.R., 2023. Remote sensing-based forest modeling reveals positive effects of functional diversity on productivity at local spatial scale. J. Geophys. Res. Biogeosciences 128 (6), e2023JG007421.
Schneider, F.D., Morsdorf, F., Schmid, B., Petchey, O.L., Hueni, A., Schimel, D.S., Schaepman, M.E., 2017. Mapping functional diversity from remotely sensed morphological and physiological forest traits. Nature Commun. 8 (1).
Shannon, C.E., 1948. A mathematical theory of communication. Bell Syst. Tech. J. 27 (3), 379–423.
Shi, Y., Skidmore, A.K., Wang, T., Holzwarth, S., Heiden, U., Pinnel, N., Zhu, X., Heurich, M., 2018. Tree species classification using plant functional traits from LiDAR and hyperspectral data. Int. J. Appl. Earth Obs. Geoinf. 73, 207–219.
Silveira, E.M., Radeloff, V.C., Martinuzzi, S., Pastur, G.J.M., Rivera, L.O., Politi, N., Lizarraga, L., Farwell, L.S., Elsen, P.R., Pidgeon, A.M., 2021. Spatio-temporal remotely sensed indices identify hotspots of biodiversity conservation concern. Remote Sens. Environ. 258, 112368.
Simpson, E.H., 1949. Measurement of diversity. nature 163 (4148), 688.
Stirling, G., Wilsey, B., 2001. Empirical relationships between species richness, evenness, and proportional diversity. Amer. Nat. 158 (3), 286–299.
Svoboda, J., Štych, P., Laštovička, J., Paluba, D., Kobliuk, N., 2022. Random forest classification of land use, land-use change and forestry (LULUCF) using sentinel-2 data—A case study of Czechia. Remote Sens. 14 (5), 1189.
Toledo, V.M., et al., 2001. Indigenous peoples and biodiversity. Encycl. Biodivers. 3, 451–463.
Torresani, M., Rocchini, D., Sonnenschein, R., Zebisch, M., Hauffe, H.C., Heym, M., Pretzsch, H., Tonon, G., 2020. Height variation hypothesis: A new approach for estimating forest species diversity with CHM LiDAR data. Ecol. Indic. 117, 106520.
Wallis, C.I., Crofts, A.L., Inamdar, D., Arroyo-Mora, J.P., Kalacska, M., Laliberté, É., Vellend, M., 2023. Remotely sensed carbon content: The role of tree composition and tree diversity. Remote Sens. Environ. 284, 113333.
Wang, R., Gamon, J.A., 2019. Remote sensing of terrestrial plant biodiversity. Remote Sens. Environ. 231, 111218.
Xi, Y., Zhang, W., Brandt, M., Tian, Q., Fensholt, R., 2023. Mapping tree species diversity of temperate forests using multi-temporal sentinel-1 and -2 imagery. Sci. Remote Sens. 8, 100094.
Zhao, Y., Zeng, Y., Zheng, Z., Dong, W., Zhao, D., Wu, B., Zhao, Q., 2018. Forest species diversity mapping using airborne LiDAR and hyperspectral data in a subtropical forest in China. Remote Sens. Environ. 213, 104–114.
Zheng, Z., Schmid, B., Zeng, Y., Schuman, M.C., Zhao, D., Schaepman, M.E., Morsdorf, F., 2023. Remotely sensed functional diversity and its association with productivity in a subtropical forest. Remote Sens. Environ. 290, 113530.
Zhu, X., Skidmore, A.K., Wang, T., Liu, J., Darvishzadeh, R., Shi, Y., Premier, J., Heurich, M., 2018. Improving leaf area index (LAI) estimation by correcting for clumping and woody effects using terrestrial laser scanning. Agricult. Forest Meteorol. 263, 276–286.
Zupanc, A., 2017. Improving cloud detection with machine learning. 10, p. 2019, Accessed: Oct.